



Figure 1: Demonstration of the proposed method.

# PRIOR-BASED 4D HUMAN-SCENE RECONSTRUCTION FROM MONOCULAR VIDEOS

Anonymous authors

Paper under double-blind review

## ABSTRACT

Accurately capturing dynamic humans as they interact with their 3D environment from a single camera is a pivotal goal for applications spanning from assistive robotics to AR. However, current monocular approaches fall short, as they are typically restricted to reconstructing either the person or the static background in isolation. Methods that capture both often rely on cumbersome multi-view setups, limiting their real-world applicability. To this end, we propose a novel framework that reconstructs the complete 4D human-scene representation from monocular video. We formulate the task as an ill-posed inverse problem and introduce a robust regularization strategy that leverages two complementary priors: a static 3D Gaussian Splatting representation of the scene, and an animatable, SMPL-based 3D Gaussian avatar of the human. Our method jointly optimizes the camera pose, human motion, and the parameters of both priors to faithfully reconstruct time-varying geometry, appearance, and physically plausible human-scene interactions. We validate our approach on a self-collected dataset featuring synchronized human acting videos, human and scene scan videos. Our results demonstrate state-of-the-art performance, achieving average 23 dB PSNR on challenging novel views and surpassing existing monocular baselines.

## 1 INTRODUCTION

From autonomous service robots and AR navigation to telepresence and sports broadcasting, many everyday applications rely on perceiving human activities in context. Effective interaction requires not only recognizing what people are doing, but also understanding the 3D layout of the surrounding environment and how people move and make contact with it over time. This motivates 4D human-scene reconstruction, jointly recovering the time-varying geometry, appearance, and motion of humans and scenes, along with their spatial relationships. To be practical and cost-effective beyond controlled studios, the method should generalize across individuals, clothing, and environments, and operate on monocular RGB videos captured with smartphones. However, existing approaches often focus only on the human Qian et al. (2024); Hu et al. (2024b) or the static scene Xu et al. (2024a); Wen et al. (2025), or assume multi-view synchronized cameras and extensive calibration Xu et al. (2024b); Wang et al. (2025), limiting applicability in real-world settings.

054 Although existing monocular 4D human-scene reconstruction method Zhang et al. (2025); Kim  
055 et al. (2025); Moon et al. (2024a) are successful in their respective tasks, the challenge remains  
056 in generalizing to novel viewpoints outside the input camera trajectory. Some artifacts may be  
057 produced, such as the elongated 3D Gaussian oaters in scenes or the opacity leakage and wrong  
058 SMPL pose of humans. It's caused by the fact that the monocular 4D human-scene reconstruction  
059 problem is naturally ill-posed with multiple valid solutions, which means even if the rendered results  
060 appear realistic at the training view, they can still correspond to the inaccurate spatial geometry and  
061 appearance features of the avatar and scene representations. Consequently, there is a growing need  
062 for methods that reconstruct humans and scenes from monocular videos and deliver faithful novel  
063 view rendering in everyday scenarios.

064 Following the approach to address ill-posed problems by mathematicians Bertero et al. (1988), we  
065 propose a novel method that integrates scene and human priors as regularization to transform the  
066 ill-posed problem into well-posed approximations. By incorporating priors, the optimization of the  
067 canonical avatar and scene becomes relatively tractable, and the complex problem of modeling point  
068 motions is reformulated as estimating SMPL parameters along with the corresponding deformations.

069 As shown in Fig. 2, our framework rst extracts two complementary priors: a static scene prior from  
070 a scene-scan video using 3D Gaussian Splatting Kerbl et al. (2023), and an animatable human prior  
071 from a human-scan video via an SMPL-based 3D Gaussian avatar reconstruction model Moon et al.  
072 (2024a). These priors serve as regularization, enabling a monocular acting video to be used for camera  
073 tracking, human pose estimation, and dense photorealistic reconstruction of both the scene and  
074 the human. However, directly combining these priors presents three challenges: First, monocular  
075 reconstructions suffer from scale ambiguity, leading to mismatched scales between the avatar and  
076 the scene. Naive integration often results in oating humans or penetrations; Second, clothing is  
077 inherently deformable, and pose-dependent non-rigid deformations such as folds cannot be captured  
078 by a xed avatar model; Third, since all three input videos are recorded on smartphones, appear-  
079 ance discrepancies arise between the priors and the acting video, producing color inconsistencies in  
080 reconstruction which may destroy the geometric consistency.

081 To address these issues, we design three targeted solutions. For the rst challenge, we introduce an  
082 optimizable parameter to adjust avatar size, and a contact loss to enforce spatial contact between  
083 human and scene. For the second challenge, we augment the SMPL avatar with pose-dependent  
084 offsets and incorporate a normal loss to better capture clothing related deformations. For the third  
085 challenge, we optimize only the appearance features of the scene, together with the captured camera  
086 poses, preventing over tting of geometry to training views and preserving geometric consistency.  
087 For training and evaluation, We construct a dataset that includes six static scenes, four human scan  
088 sequences, and six acting videos, with three additional sequences exclusively for evaluation. On  
089 novel viewpoint rendering, our approach attains an average PSNR of 23.5 dB, outperforming the  
090 baseline by 3 dB.

091 In summary, our contributions are:

- 092 • A novel method is proposed to solve the novel view synthesis challenges of 4D human-scene  
093 reconstruction in the wild by introducing scene and avatar priors.
- 094 • We refine the priors through the 2D/3D knowledge extracted from the monocular acting video.
- 095 • We collect a real-world dataset consisting of acting videos paired with additional human and scene  
096 scans. The effectiveness of our method is evaluated by extensive ablation studies and comparisons.

## 098 2 RELATED WORKS

### 100 2.1 DYNAMIC RECONSTRUCTION

101  
102 To reconstruct dynamic scenes, several works, such as D-NeRF Pumarola et al. (2021) and Hy-  
103 perReel Attal et al. (2023), leverage implicit representations to model time-varying radiance elds  
104 but suffer from high computational costs and slow convergence. Voxel-based approaches like Hex-  
105 Plane Cao & Johnson (2023) and V4D Gan et al. (2023) improve ef ciency through 4D grid factor-  
106 ization, yet they struggle to balance resolution with memory constraints. In contrast, 3D Gaussian  
107 Splatting Kerbl et al. (2023) offers real-time rendering and explicit geometric control, making it  
a promising candidate for dynamic extensions. Building on this momentum, several works have

sought to extend Gaussian-based methods to model temporal dynamics. Luiten et al. (2024) introduced a foundational framework for persistent dynamic view synthesis by tracking 3D Gaussians over time. Concurrently, Yang et al. (2024b), Wu et al. (2024b), and Liang et al. (2023) proposed joint optimization strategies that couple canonical-space Gaussians with deformation fields to disentangle geometry and motion. These approaches implicitly assume topological consistency by anchoring dynamics to a static canonical configuration, limiting their applicability to scenes with rigid or semi-rigid motions. Kratimenos et al. (2024) further decomposed motion into neural trajectories to enforce locality and rigidity priors, enhancing robustness for monocular video inputs. While in various dynamic scenarios, these methods achieve compelling rendering results on viewpoints that lie within the training trajectory, they can struggle with maintaining geometric consistency when rendered under out-of-distribution poses.

## 2.2 ANIMATABLE 3D HUMAN AVATARS

The creation of animatable 3D human avatars has advanced significantly through diverse 3D representations and learning frameworks. Early works leveraged parametric meshes, such as SMPL, extended via per-vertex offsets Alldieck et al. (2018) or driven by conditional variational autoencoders Bagautdinov et al. (2021). Localized representations, like texel-aligned features Remelli et al. (2022), improved detail preservation. The advent of neural radiance fields (NeRF) Mildenhall et al. (2021) spurred volumetric approaches, enabling high-fidelity avatars from multi-view studio captures Peng et al. (2021a;b); Shen et al. (2023). Concurrently, methods like Kwon et al. (2021) incorporated vertex-aligned features for enhanced generalization. Recent efforts prioritize monocular video inputs, circumventing the need for 3D supervision (e.g., Jiang et al. (2022), Guo et al. (2023), and Jiang et al. (2023)). The rise of 3D Gaussian Splatting (3DGS) Kerbl et al. (2023) further accelerated progress, enabling efficient rendering in avatars via triplane decomposition Kocabas et al. (2024), SMPL-aligned positional maps Hu et al. (2024a), or expressive Gaussian-based models Liu et al. (2024). Despite these advances, most methods focus on body motion, neglecting hand and facial animation. While X-Avatar Shen et al. (2023) supports whole-body animation, it requires extensive 3D-registered facial data and struggles with in-the-wild monocular videos. Similarly, Liu et al. (2024) lack facial expression control. Parametric models like SMPL-X Pavlakos et al. (2019) unify body, face, and hands, inspiring pose estimation methods Choutas et al. (2020); Moon et al. (2022), yet translating these to expressive, lightweight avatars remains challenging. Hand-specific models, such as UHM Moon et al. (2024b) and its relightable extension Chen et al. (2024), highlight the complexity of part-specific modeling, underscoring the need for holistic, practical solutions. However, these methods generally focus only on the reconstruction of an animatable avatar in the canonical space alone, with the static scene being largely overlooked.

## 2.3 HUMAN-SCENE RECONSTRUCTION

The field of human-scene reconstruction has rapidly progressed from independent reconstructions of humans and environments toward unified frameworks that jointly recover dynamic human motion and surrounding scenes with neural representation Kim et al. (2025); Xue et al. (2024); Zhang et al. (2025); Moon et al. (2024a); Liu et al. (2025). JOSH Liu et al. (2025) initializes with local scene reconstruction and human mesh recovery, and subsequently performs joint optimization of human motion and scene geometry under human-scene contact constraints. Showmak3r Kim et al. (2025) reconstructs dynamic radiance fields from TV shows, facilitating scene editing analogous to operations in a production control room. Furthermore, the method incorporates Score Distillation Sampling Loss Lee et al. (2024) to alleviate artifacts that typically appear in novel viewpoints. ODHSR Zhang et al. (2025) leverages monocular RGB videos of humans to jointly reconstruct a dense photorealistic Gaussian representation of both the scene and the dynamic human, and simultaneously recover camera poses, human motion, and human silhouettes under a SLAM formulation. HSR Xue et al. (2024) and Exavatar Moon et al. (2024a) are the most closely related works to ours. HSR jointly optimizes dynamic human and scene geometry using neural implicit representations, with supervision provided by monocular depth and surface normals estimated from full-frame predictions. However, it often fails to faithfully capture human motion from novel viewpoints. Similar to our approach, Exavatar leverages 3D Gaussians to represent both the full-body human avatar and the surrounding scene. Nevertheless, it often produces geometric inconsistencies in the scene and suffers from opacity leakage artifacts in the avatar.

162  
163  
164  
165  
166  
167  
168  
169  
170  
171  
172  
173  
174  
175  
176  
177  
178  
179  
180  
181  
182  
183  
184  
185  
186  
187  
188  
189  
190  
191  
192  
193  
194  
195  
196  
197  
198  
199  
200  
201  
202  
203  
204  
205  
206  
207  
208  
209  
210  
211  
212  
213  
214  
215

Figure 2: This is the pipeline of our method. Given an acting video, this model first extract the SMPL-X parameter used to drive and localize the avatar prior in the scene prior. Then we perform photometric, normal loss as 2D supervision, contact and regularization loss as 3D supervision to optimize jointly the camera pose, human motion, and the parameters of both priors. After optimization, the output representation can achieve realistic novel view synthesis.

### 3 PRELIMINARIES

Prior-based 4D human-scene Gaussian reconstruction involves both static scene and dynamic human reconstruction. We introduce preliminaries of these two tasks in Sec.3.1 and Sec.3.2, respectively.

#### 3.1 STATIC SCENE PRIOR RECONSTRUCTION(GS SCENE)

Our goal is to obtain a dense reconstruction of the static background from a scene-scan video. Following 3D Gaussian Splatting (3DGS) Kerbl et al. (2023), we explicitly represent the background as a set of  $M$  anisotropic Gaussians in the world frame  $\mathcal{G} = \{ (V_{b,i}; \alpha_{b,i}; S_{b,i}; R_{b,i}; z_{b,i}) \}_{i=1}^{M_s}$ , where the center  $V_{b,i} \in \mathbb{R}^3$ , opacity  $\alpha_{b,i} \in [0, 1]$ , covariance  $S_{b,i} \in \mathbb{R}^{3 \times 3}$ , and SH appearance coefficients  $z_{b,i}$  parameterize geometry and color.

$$S_{b,i} = R_{b,i} S_{b,i} S_{b,i}^T R_{b,i}^T; \quad R_{b,i} \in \text{SO}(3); \quad S_{b,i} = \text{diag}(s_x; s_y; s_z); \quad (1)$$

Appearance is modeled with spherical harmonics (SH) to achieve view-dependent color. To obtain reliable geometry and mitigate floating-Gaussian artifacts, we supervise the rendered depth with monocular depth from Depth-Anything v2 Yang et al. (2024a) and extend the 3DGS objective with regularizers that improve surface consistency Kerbl et al. (2024). Therefore, we only optimize its SH parameters in the subsequent optimization process, as described in Sec.1.

#### 3.2 ANIMATABLE HUMAN AVATAR

Our goal is to obtain a fully drivable human avatar model from a single-person scan video. To faithfully capture fine details and achieve photorealistic rendering, the avatar must support whole-body drivability, including the body, hands, and facial expressions. For this purpose, we adopt the off-the-shelf method ExAvatar Moon et al. (2024a) for the Gaussian avatar reconstruction.

Unlike conventional Gaussian representations that use ellipsoids with opacity and spherical harmonic (SH) coefficients, the formulation is simplified by representing each Gaussian as a solid sphere with direct RGB values for appearance to avoid serious overfitting. In the canonical space, the neutral posed avatar is parameterized as a set of optimizable variables  $\mathcal{G} = \{ (V_{h,i}; S_{h,i}; C_{h,i}) \}_{i=1}^{M_h}$ , where shape vector  $V_{h,i} \in \mathbb{R}^3$ , global scale  $S_{h,i} \in \mathbb{R}$ , 3D position  $V_{h,i} \in \mathbb{R}^3$ , scale  $S_{h,i} \in \mathbb{R}$ , and RGB color  $C_{h,i} \in \mathbb{R}^3$ .

216  
217  
218  
219  
220  
221  
222  
223  
224  
225  
226  
227  
228  
229  
230  
231  
232  
233  
234  
235  
236  
237  
238  
239  
240  
241  
242  
243  
244  
245  
246  
247  
248  
249  
250  
251  
252  
253  
254  
255  
256  
257  
258  
259  
260  
261  
262  
263  
264  
265  
266  
267  
268  
269

Figure 3: Qualitative ablation of Regularization Loss. The regularization significantly reduces artifacts at both train and novel views.

Figure 4: Qualitative ablation of  $J_{\text{contact}}$ . The corner inset illustrates the human-scene contact situation.

## 4 METHOD

In this section, we first formalize the overall 4D human-scene reconstruction framework in Sec. 4.1. Then the initialization process is proposed in Sec. 4.2. After that, we address how to accurately deform the avatar and localize the avatar within the scene in Sec. 4.3. Finally, we describe the optimization method in Sec. 4.4.

### 4.1 PROBLEM SETUP

To solve the 4D human-scene Gaussian reconstruction problem, we need to reconstruct three key components: the static scene, animatable avatar and whole-body driving signals. The inputs consist of two monocular scanning videos for constructing the scene and human prior respectively, and an acting video for human-scene joint reconstruction. The output is a Gaussian representation of the static scene  $G$  and a canonical Gaussian asset of the animatable avatar  $A$ . The SMPL-X driving signals  $\{E^t; P_c^t; t; g_{t=0}^M\}$ , where  $\{E^t; P_c^t; t\}$  represents the 3D joint poses of the SMPL-X model,  $g_{t=0}^M$  denotes the facial expression parameters, and  $M$  is the total number of frames in the acting video.

### 4.2 INITIALIZATION

From the acting video, we extract frames and apply off-the-shelf models to regress SMPL-X and FLAME parameters, as well as 2D keypoint annotations Contributors (2020). These are then jointly optimized to achieve alignment with the detected keypoints.

To further ground the avatar in the scene, we extract 3D ground points from the scene prior with masks predicted by the Segment Anything Model Ren et al. (2024) and fit a plane  $\vec{x} \cdot \vec{nd} = 0$  using RANSAC. The estimated plane provides the initial global scale factor  $\alpha_0$  for human-scene contact. The final output is the optimized SMPL-X parameter set  $\{s; f; P_c^t; t; g_{t=0}^M\}$ ; where  $s$  is the shape parameter of the SMPL model. Camera poses in the scene prior’s coordinate system are estimated by segmenting the human foreground with Segment Anything Ren et al. (2024) and applying structure-from-motion (SfM) Sarlin et al. (2019) jointly to obtain both a sparse scene point cloud and initial acting camera poses. For supervising fine-grained surface geometry, especially clothing deformations, we employ the human surface normal foundation model Khirodkar et al. (2024) to generate per-frame normal maps from the acting video, which are used as ground-truth normals  $N$  during optimization.

270  
271  
272  
273  
274  
275  
276  
277  
278  
279  
280  
281  
282  
283  
284  
285  
286  
287

Figure 5: Qualitative ablation of avatar and scene priors.

288  
289  
290  
291

Figure 6: Qualitative ablation study of  $I_{\text{normal}}$  from a novel evaluation view rendering of the avatar, with comparisons against the baseline method.

292  
293  
294  
295

### 4.3 AVATAR LOCATOR AND RENDERING

296  
297  
298  
299  
300  
301  
302

#### 4.3.1 AVATAR DEFORMATION AND LOCALIZATION

To model the deformation and movements of human, we drive the avatar's 3D Gaussian assets from canonical space to posed space using SMPL-X signals. Given the neutral posed vertex positions  $V_h = V_h(\cdot)$ , we first apply the per-frame expression code to produce expression dependent offsets on facial vertices. To capture clothing in the canonical space, we introduce an id-dependent cloth offset  $V_{\text{cloth}}$  specific for avatar, and a pose-dependent offset  $V_{\text{pose}}(\cdot)$  that models deformation. The similar operation is applied to the scaling matrices. The vertices in the camera coordinate are then obtained via linear blend skinning (LBS) under pose

303  
304  
305

$$V_h^t = V_h + V_{\text{expr}}(\cdot) + V_{\text{cloth}} + V_{\text{pose}}(\cdot); \quad (2)$$

306  
307  
308

$$V_{h;\text{cam}}^t = \text{LBS}(V_h^t; \cdot; W); \quad (3)$$

Finally, we transform the avatar from the camera coordinate system to the world using the camera extrinsic parameters  $V_{h;\text{world}} = E^t V_{h;\text{cam}}^t$ ; enabling composition with the static scene.

309

#### 4.3.2 RENDERING

310  
311

The rendering of the model at a specified camera pose is achieved using the 3D Gaussian splatting pipeline Kerbl et al. (2023):

312  
313  
314

$$\hat{I} = \sum_{k=1}^K T^k c^k; \quad \text{where } T^k = \prod_{j=1}^M (1 - \alpha_j) \quad (4)$$

315  
316  
317  
318

where  $c$  represents the RGB color value of each vertex. Following Liang et al. (2024), we also perform volume rendering on the avatar's normal vectors to obtain a 2D normal map for each frame. The spatial normals are computed from the mesh structure defined by the supplied faces and the vertex positions in the camera coordinate system.

319  
320  
321  
322

$$\hat{N} = \sum_{k=1}^K T^k n^k; \quad \text{where } n^k = \text{Normal}(V_{h;\text{cam}}^t; F) \quad (5)$$

323

where  $F$  represents the mesh face of SMPL-X human model.

324  
325  
326  
327  
328  
329  
330  
331  
332  
333  
334  
335  
336  
337  
338  
339  
340  
341  
342  
343  
344  
345  
346  
347  
348  
349  
350  
351  
352  
353  
354  
355  
356  
357  
358  
359  
360  
361  
362  
363  
364  
365  
366  
367  
368  
369  
370  
371  
372  
373  
374  
375  
376  
377

#### 4.4 OPTIMIZATION

##### 4.4.1 PHOTOMETRIC LOSS

To achieve more realistic rendering results, we employed widely used 2D supervision metrics in computer vision, including the L1 loss of RGB values, D-SSIM and LPIPS. These loss functions are separately applied to the Gaussian representations of both avatar and scene, using masks  $M$  provide acting video segmentation as the ground truth.

##### 4.4.2 NORMAL LOSS

In 4D reconstruction, pure photometric supervision would encourage solutions that ignore geometry, according to the fact that distinct motions can produce identical renderings. It will trap the optimization in spurious local minima. Based on this insight, we exclusively leverage normal maps to supervise the vertex positions of the avatar after deformation and LBS, ensuring the reconstructed avatar has both accurate surface details and consistent geometric structure. Inspired by Xue et al. (2024), we employ a linear combination of L1 and cosine losses of normal rendering, which together define the overall normal loss.

$$L_{\text{normal}} = \sum_1 \|\hat{N} - N\|_1 + \sum_1 |1 - \hat{N} \cdot N| \quad (6)$$

##### 4.4.3 CONTACT LOSS

For clarity, this work considers a simplified but commonly encountered scenario where the avatar's feet are assumed to remain in contact with the ground. Therefore, avatar's contact points are constrained to the vertices bound at the foot joint. We compute the distances from all foot vertices to the ground plane and select the closest  $N_{\text{contact}}$  points as contact candidates  $V_{\text{contact}}$ . To prevent the avatar from either floating above the scene or penetrating the ground, we introduce the contact terms:

$$L_{\text{contact}} = \sum_{V_{\text{contact}}} \max(0; |n \cdot V_{\text{contact}}| + d_j - c) \quad (7)$$

where  $c = 0.02$ . As describe in Sec.4.2, we has estimated the plane model  $\pi$ , which can be held constant during optimization as the scene geometry remains fixed throughout the optimization.

##### 4.4.4 REGULARIZATION LOSS

Since the captured views are limited, some body regions would never be observed. To prevent the avatar from over fitting to the observed views and corrupting unseen areas, we directly regularize the avatar's 3D assets.

Unlike traditional avatar methods that rely only on a naked-body mesh prior, we have a high-fidelity scanned avatar prior. Therefore, we introduce the Huber loss that minimizes the difference between the optimized 3D human Gaussians and corresponding prior in both color and scale.

With this formulation, the loss could naturally prevent unreasonable changes in unseen regions, thereby reducing artifacts in views outside the training cameras. As illustrated in Fig. 3, without this loss, the colors of unseen regions, such as the back and the palm become corrupted after the optimization. In contrast, when the loss is applied, the optimized model is able to maintain plausible colors even in unseen regions. Moreover, in the training views, the absence of this loss leads to opacity leakage in regions such as the neck and face.

## 5 EXPERIMENTS

### 5.1 SETUP

#### 5.1.1 DATASETS

Our method requires human and scene priors captured from scanned videos. However, to the best of our knowledge, no suitable datasets are publicly available. Therefore, we recorded six sequences by ourselves, including six different static scenes, four human scanning videos, and six acting videos.

378  
379  
380  
381  
382  
383  
384  
385  
386  
387  
388  
389  
390  
391  
392  
393  
394  
395  
396  
397  
398  
399  
400  
401  
402  
403  
404  
405  
406  
407  
408  
409  
410  
411  
412  
413  
414  
415  
416  
417  
418  
419  
420  
421  
422  
423  
424  
425  
426  
427  
428  
429  
430  
431

Figure 7: Qualitative 4D human-scene reconstruction results

Each acting video is approximately 15 to 25s long, with a frame rate of 10Hz. All of the frames are used for both training and testing. To quantitatively evaluate the model's ability of novel view synthesis, we recorded an additional evaluation video at a fixed camera pose while recording three of the acting video, providing the ground truth image at the novel view.

### 5.1.2 METRICS

We report quantitative results using three standard metrics at the evaluation view: Peak Signal-to-Noise Ratio(PSNR), Structure Similarity Index Measure(SSIM) and Learned Perceptual Image Patch and Similarity(LPIPS) Zhang et al. (2018). In addition, we introduced the Normal Mean Angle Error and the Normal Median Angle Error using the normal map obtained from sapiens Khirodkar et al. (2024) as the ground truth to quantitatively evaluate the geometry of the avatar. We also calculate the Mask IoU at the evaluation view to verify whether the avatar is localized in the correct 3D position and pose.

### 5.1.3 BASELINES

We compare our methods with the state-of-the-art 4D reconstruction methods: 4D Gaussian Wu et al. (2024a)(Template Free), HSR Xue et al. (2024) (Neural Rendering-based) and ExAvatar Moon et al. (2024a)(Gaussian Splatting-based). For a fair comparison, we disabled our camera re-orientation module, since both 4D Gaussian and ExAvatar operate with fixed camera poses without optimization. We adopt baselines' own pre-process methods if provided, but ours if not.

## 5.2 EVALUATION ON THE DATASET

We evaluate 4D Gaussians, HSR, and ExAvatar on three datasets that provide additional evaluation videos, and report rendering results from novel viewpoints.

As a hybrid representation combining 3D Gaussians and meshes, ExAvatar can realistically capture facial expressions and body movements, leading to avatar reconstruction results comparable to ours. However, as shown in Fig. 7, when rendering multi-frame sequences of both the scene and humans from novel viewpoints, ExAvatar exhibits noticeable artifacts. Specifically, opacity leakage occurs in the avatar, particularly in the face and upper body regions in scenes (a) and (b). In all tested scenes, ExAvatar also suffers from interpenetration between the avatar and the static environment, due to the lack of joint optimization of geometry. Moreover, in scene (c), the reconstructed environment contains numerous large floaters. It is caused by the lack of visual features on the gray background wall. As shown in Fig. 8, HSR incorporates monocular depth and normal priors during optimization and continually adjusts their relative scales, which helps to avoid interpenetration artifacts. However,

Table 1: Quantitative comparison with baselines at evaluation view. Lower is better except PSNR(").

Method	PSNR "	D-SSIM #	LPIPS #
4D Gaussian Wu et al. (2024a)	16.72	0.62	0.55
HSR Xue et al. (2024)	20.46	0.51	0.53
Exavatar Moon et al. (2024a)	20.38	0.38	0.41
Ours	23.57	0.30	0.27

Table 2: Quantitative comparison on the Normal Angle Error of monocular 4D human-scene reconstruction. Table 3: Quantitative comparison on the Mask IoU of monocular 4D human-scene reconstruction.

Method	Mean #	Median #
Exavatar	41.34	31.94
Ours	23.64	13.54
Ours w/o $L_{\text{normal}}$	36.03	25.52

Method	Mask IoU "
Ours	0.91
Ours w/o $L_{\text{contact}}$	0.78

the reconstructed human motions are still significantly distorted, particularly in the second scene. In addition, the rendered scenes from HSR fail to capture the details of complex textures on the ground. In the first scene, HSR is also unable to reliably distinguish between static and dynamic human, resulting in outliers in background regions without avatar.

4D Gaussians, as a template-free approach, can faithfully reconstruct static scenes. Nevertheless, it fails to properly model human appearance and motion in a canonical space, leading to poor performance under novel view synthesis.

In quantitative evaluations, our approach achieves consistently superior performance over all three baselines across standard metrics, including PSNR, SSIM, and LPIPS, as shown in Table 1.

### 5.3 ABLATION STUDIES

As shown in Fig. 5, removing the avatar prior leads to noticeable color bleeding in unseen regions and erroneous SMPL-X parameter estimation of the hand. In addition, removing the scene prior results in sparse static scene point clouds and opacity leakage, especially when rendering from novel viewpoints. These observations confirm the importance of incorporating scene and human priors for complete 4D human-scene reconstruction.

Qualitatively, as presented in Fig. 6, the absence of normal supervision severely degrades the geometric quality of the avatar and incorporating the normal loss significantly enhances geometric reconstruction under novel view synthesis and reduces the Normal Angular Error, as illustrated in Table 2. Qualitatively, as shown in Fig.4, the absence of contact constraints results in interpenetration between the human and the scene. Quantitatively, incorporating the contact loss significantly improves Mask IoU under novel view synthesis, as shown in Table3, thereby ensuring a correct 3D spatial relationship between the human and the scene.

## 6 CONCLUSION

In conclusion, we propose a novel framework for complete 4D human-scene reconstruction from monocular videos, addressing the limitations of prior methods and enabling faithful novel-view synthesis. Our method jointly optimizes camera poses, human motion, and scene geometry by introducing a regularization strategy and combining static 3D Gaussian scene representation with an animatable SMPL-based avatar. Experimental results demonstrate that our approach recovers time-varying geometry and appearance, achieving state-of-the-art performance and significantly outperforming existing monocular baselines.

## REFERENCES

- 486  
487  
488 Thiemo Alldieck, Marcus Magnor, Weipeng Xu, Christian Theobalt, and Gerard Pons-Moll. Video  
489 based reconstruction of 3d people models. In Proceedings of the IEEE Conference on Computer  
490 Vision and Pattern Recognition, pp. 8387–8397, 2018.
- 491 Benjamin Attal, Jia-Bin Huang, Christian Richardt, Michael Zollhoefer, Johannes Kopf, Matthew  
492 O’Toole, and Changil Kim. Hyperreel: High- delity 6-dof video with ray-conditioned sampling.  
493 In Proceedings of the IEEE/CVF Conference on Computer Vision and Pattern Recognition, pp.  
494 16610–16620, 2023.
- 495  
496 Timur Bagautdinov, Chenglei Wu, Tomas Simon, Fabian Prada, Takaaki Shiratori, Shih-En Wei,  
497 Weipeng Xu, Yaser Sheikh, and Jason Saragih. Driving-signal aware full-body avatars. *ACM*  
498 *Transactions on Graphics (TOG)*, 40(4):1–17, 2021.
- 499 Mario Bertero, Tomaso A Poggio, and Vincent Torre. Ill-posed problems in early vision. *Proceed-*  
500 *ings of the IEEE*, 76(8):869–889, 1988.
- 501  
502 Ang Cao and Justin Johnson. Hexplane: A fast representation for dynamic scenes. In Proceedings  
503 of the IEEE/CVF Conference on Computer Vision and Pattern Recognition, pp. 130–141, 2023.
- 504  
505 Zhaoxi Chen, Gyeongsik Moon, Kaiwen Guo, Chen Cao, Stanislav Pidhorskyi, Tomas Simon, Ro-  
506 han Joshi, Yuan Dong, Yichen Xu, Bernardo Pires, et al. Urhand: Universal relightable hands.  
507 In Proceedings of the IEEE/CVF Conference on Computer Vision and Pattern Recognition, pp.  
508 119–129, 2024.
- 509 Vasileios Choutas, Georgios Pavlakos, Timo Bolkart, Dimitrios Tzionas, and Michael J Black.  
510 Monocular expressive body regression through body-driven attention. In *Computer Vision–ECCV*  
511 *2020: 16th European Conference, Glasgow, UK, August 23–28, 2020, Proceedings, Part X 16*,  
512 pp. 20–40. Springer, 2020.
- 513  
514 MMPose Contributors. Openmmlab pose estimation toolbox and benchmark. [https://github.](https://github.com/open-mmlab/mmpose)  
515 [com/open-mmlab/mmpose](https://github.com/open-mmlab/mmpose), 2020.
- 516  
517 Wanshui Gan, Hongbin Xu, Yi Huang, Shifeng Chen, and Naoto Yokoya. V4d: Voxel for 4d novel  
518 view synthesis. *IEEE Transactions on Visualization and Computer Graphics*, 30(2):1579–1591,  
519 2023.
- 520  
521 Chen Guo, Tianjian Jiang, Xu Chen, Jie Song, and Otmar Hilliges. Vid2avatar: 3d avatar recon-  
522 struction from videos in the wild via self-supervised scene decomposition. In Proceedings of the  
523 IEEE/CVF Conference on Computer Vision and Pattern Recognition, pp. 12858–12868, 2023.
- 524  
525 Liangxiao Hu, Hongwen Zhang, Yuxiang Zhang, Boyao Zhou, Boning Liu, Shengping Zhang, and  
526 Liqiang Nie. Gaussianavatar: Towards realistic human avatar modeling from a single video via  
527 animatable 3d gaussians. In Proceedings of the IEEE/CVF conference on computer vision and  
528 pattern recognition, pp. 634–644, 2024a.
- 529  
530 Shoukang Hu, Tao Hu, and Ziwei Liu. Gauhuman: Articulated gaussian splatting from monocular  
531 human videos. In Proceedings of the IEEE/CVF conference on computer vision and pattern  
532 recognition, pp. 20418–20431, 2024b.
- 533  
534 Tianjian Jiang, Xu Chen, Jie Song, and Otmar Hilliges. Instantavatar: Learning avatars from monoc-  
535 ular video in 60 seconds. In Proceedings of the IEEE/CVF Conference on Computer Vision and  
536 Pattern Recognition, pp. 16922–16932, 2023.
- 537  
538 Wei Jiang, Kwang Moo Yi, Golnoosh Samei, Oncel Tuzel, and Anurag Ranjan. Neuman: Neural  
539 human radiance eld from a single video. In *European Conference on Computer Vision*, pp.  
402–418. Springer, 2022.
- Bernhard Kerbl, Georgios Kopanas, Thomas Laitner, and George Drettakis. 3d gaussian splat-  
ting for real-time radiance eld rendering. *ACM Transactions on Graphics*, 42(4), July 2023.  
URL <https://repo-sam.inria.fr/fungraph/3d-gaussian-splatting/>.

- 540 Bernhard Kerbl, Andreas Meuleman, Georgios Kopanas, Michael Wimmer, Alexandre Lanvin, and  
541 George Drettakis. A hierarchical 3d gaussian representation for real-time rendering of very large  
542 datasets. *ACM Transactions on Graphics*, 43(4), July 2024. URL <https://repo-sam.inria.fr/fungraph/hierarchical-3d-gaussians/>.  
543
- 544 Rawal Khrodar, Timur Bagautdinov, Julieta Martinez, Su Zhaoen, Austin James, Peter Selednik,  
545 Stuart Anderson, and Shunsuke Saito. Sapiens: Foundation for human vision models. In *European Conference on Computer Vision*, pp. 206–228. Springer, 2024.  
546
- 547 Sangmin Kim, Seunguk Do, and Jaesik Park. Showmak3r: Compositional tv show reconstruction.  
548 In *Proceedings of the Computer Vision and Pattern Recognition Conference*, pp. 864–874, 2025.  
549
- 550 Muhammed Kocabas, Jen-Hao Rick Chang, James Gabriel, Oncel Tuzel, and Anurag Ranjan. Hugs:  
551 Human gaussian splats. In *Proceedings of the IEEE/CVF conference on computer vision and  
552 pattern recognition*, pp. 505–515, 2024.  
553
- 554 Agelos Kratimenos, Jiahui Lei, and Kostas Daniilidis. Dynmf: Neural motion factorization for real-  
555 time dynamic view synthesis with 3d gaussian splatting. In *European Conference on Computer  
556 Vision*, pp. 252–269. Springer, 2024.  
557
- 558 Youngjoong Kwon, Dahun Kim, Duygu Ceylan, and Henry Fuchs. Neural human performer: Learn-  
559 ing generalizable radiance fields for human performance rendering. *Advances in Neural Informa-  
560 tion Processing Systems*, 34:24741–24752, 2021.  
561
- 562 Inhee Lee, Byungjun Kim, and Hanbyul Joo. Guess the unseen: Dynamic 3d scene reconstruction  
563 from partial 2d glimpses. In *Proceedings of the IEEE/CVF conference on computer vision and  
564 pattern recognition*, pp. 1062–1071, 2024.
- 565 Yiqing Liang, Numair Khan, Zhengqin Li, Thu Nguyen-Phuoc, Douglas Lanman, James Tompkin,  
566 and Lei Xiao. Gaufré: Gaussian deformation fields for real-time dynamic novel view synthesis.  
567 *arXiv preprint arXiv:2312.11458*, 2023.  
568
- 569 Zhihao Liang, Qi Zhang, Ying Feng, Ying Shan, and Kui Jia. Gs-ir: 3d gaussian splatting for  
570 inverse rendering. In *Proceedings of the IEEE/CVF Conference on Computer Vision and Pattern  
571 Recognition*, pp. 21644–21653, 2024.
- 572 Xinqi Liu, Chenming Wu, Xing Liu, Jialun Liu, Jinbo Wu, Chen Zhao, Haocheng Feng, Errui Ding,  
573 and Jingdong Wang. Gea: Reconstructing expressive 3d gaussian avatar from monocular video.  
574 *arXiv e-prints*, pp. *arXiv-2402*, 2024.  
575
- 576 Zhizheng Liu, Joe Lin, Wayne Wu, and Bolei Zhou. Joint optimization for 4d human-scene recon-  
577 struction in the wild. *arXiv preprint arXiv:2501.02158*, 2025.
- 578 Jonathon Luiten, Georgios Kopanas, Bastian Leibe, and Deva Ramanan. Dynamic 3d gaussians:  
579 Tracking by persistent dynamic view synthesis. In *2024 International Conference on 3D Vision  
580 (3DV)*, pp. 800–809. IEEE, 2024.  
581
- 582 Ben Mildenhall, Pratul P Srinivasan, Matthew Tancik, Jonathan T Barron, Ravi Ramamoorthi, and  
583 Ren Ng. Nerf: Representing scenes as neural radiance fields for view synthesis. *Communications  
584 of the ACM*, 65(1):99–106, 2021.  
585
- 586 Gyeongsik Moon, Hongsuk Choi, and Kyoung Mu Lee. Accurate 3d hand pose estimation for  
587 whole-body 3d human mesh estimation. In *Proceedings of the IEEE/CVF Conference on Com-  
588 puter Vision and Pattern Recognition*, pp. 2308–2317, 2022.
- 589 Gyeongsik Moon, Takaaki Shiratori, and Shunsuke Saito. Expressive whole-body 3d gaussian  
590 avatar. In *European Conference on Computer Vision*, pp. 19–35. Springer, 2024a.  
591
- 592 Gyeongsik Moon, Weipeng Xu, Rohan Joshi, Chenglei Wu, and Takaaki Shiratori. Authentic hand  
593 avatar from a phone scan via universal hand model. In *Proceedings of the IEEE/CVF Conference  
on Computer Vision and Pattern Recognition*, pp. 2029–2038, 2024b.

- 594 Georgios Pavlakos, Vasileios Choutas, Nima Ghorbani, Timo Bolkart, Ahmed AA Osman, Dimitrios  
595 Tzionas, and Michael J Black. Expressive body capture: 3d hands, face, and body from a single  
596 image. In *Proceedings of the IEEE/CVF conference on computer vision and pattern recognition*,  
597 pp. 10975–10985, 2019.
- 598  
599 Sida Peng, Junting Dong, Qianqian Wang, Shangzhan Zhang, Qing Shuai, Xiaowei Zhou, and Hujun  
600 Bao. Animatable neural radiance fields for modeling dynamic human bodies. In *Proceedings of*  
601 *the IEEE/CVF International Conference on Computer Vision*, pp. 14314–14323, 2021a.
- 602 Sida Peng, Yuanqing Zhang, Yinghao Xu, Qianqian Wang, Qing Shuai, Hujun Bao, and Xiaowei  
603 Zhou. Neural body: Implicit neural representations with structured latent codes for novel view  
604 synthesis of dynamic humans. In *Proceedings of the IEEE/CVF conference on computer vision*  
605 *and pattern recognition*, pp. 9054–9063, 2021b.
- 606  
607 Albert Pumarola, Enric Corona, Gerard Pons-Moll, and Francesc Moreno-Noguer. D-nerf: Neural  
608 radiance fields for dynamic scenes. In *Proceedings of the IEEE/CVF conference on computer*  
609 *vision and pattern recognition*, pp. 10318–10327, 2021.
- 610 Zhiyin Qian, Shaofei Wang, Marko Mihajlovic, Andreas Geiger, and Siyu Tang. 3dgs-avatar: Ani-  
611 matable avatars via deformable 3d gaussian splatting. In *Proceedings of the IEEE/CVF conference*  
612 *on computer vision and pattern recognition*, pp. 5020–5030, 2024.
- 613  
614 Edoardo Remelli, Timur Bagautdinov, Shunsuke Saito, Chenglei Wu, Tomas Simon, Shih-En Wei,  
615 Kaiwen Guo, Zhe Cao, Fabian Prada, Jason Saragih, et al. Drivable volumetric avatars using  
616 texel-aligned features. In *ACM SIGGRAPH 2022 conference proceedings*, pp. 1–9, 2022.
- 617 Tianhe Ren, Shilong Liu, Ailing Zeng, Jing Lin, Kunchang Li, He Cao, Jiayu Chen, Xinyu Huang,  
618 Yukang Chen, Feng Yan, Zhaoyang Zeng, Hao Zhang, Feng Li, Jie Yang, Hongyang Li, Qing  
619 Jiang, and Lei Zhang. Grounded sam: Assembling open-world models for diverse visual tasks,  
620 2024.
- 621  
622 Paul-Edouard Sarlin, Cesar Cadena, Roland Siegwart, and Marcin Dymczyk. From coarse to fine:  
623 Robust hierarchical localization at large scale. In *Proceedings of the IEEE/CVF conference on*  
624 *computer vision and pattern recognition*, pp. 12716–12725, 2019.
- 625 Kaiyue Shen, Chen Guo, Manuel Kaufmann, Juan Jose Zarate, Julien Valentin, Jie Song, and Otmar  
626 Hilliges. X-avatar: Expressive human avatars. In *Proceedings of the IEEE/CVF Conference on*  
627 *Computer Vision and Pattern Recognition*, pp. 16911–16921, 2023.
- 628  
629 Yifan Wang, Peishan Yang, Zhen Xu, Jiaming Sun, Zhanhua Zhang, Yong Chen, Hujun Bao, Sida  
630 Peng, and Xiaowei Zhou. Freetimegs: Free gaussian primitives at anytime anywhere for dynamic  
631 scene reconstruction. In *Proceedings of the Computer Vision and Pattern Recognition Conference*,  
632 pp. 21750–21760, 2025.
- 633  
634 Long Wen, Shixin Li, Yu Zhang, Yuhong Huang, Jianjie Lin, Fengjunjie Pan, Zhenshan Bing, and  
635 Alois Knoll. Gassidy: Gaussian splatting slam in dynamic environments. In *2025 IEEE Interna-*  
636 *tional Conference on Robotics and Automation (ICRA)*, pp. 8471–8477. IEEE, 2025.
- 637 Guanjun Wu, Taoran Yi, Jiemin Fang, Lingxi Xie, Xiaopeng Zhang, Wei Wei, Wenyu Liu, Qi Tian,  
638 and Xinggang Wang. 4d gaussian splatting for real-time dynamic scene rendering. In *Proceedings*  
639 *of the IEEE/CVF Conference on Computer Vision and Pattern Recognition (CVPR)*, pp. 20310–  
640 20320, June 2024a.
- 641 Guanjun Wu, Taoran Yi, Jiemin Fang, Lingxi Xie, Xiaopeng Zhang, Wei Wei, Wenyu Liu, Qi Tian,  
642 and Xinggang Wang. 4d gaussian splatting for real-time dynamic scene rendering. In *Proceed-*  
643 *ings of the IEEE/CVF conference on computer vision and pattern recognition*, pp. 20310–20320,  
644 2024b.
- 645  
646 Yueming Xu, Haochen Jiang, Zhongyang Xiao, Jianfeng Feng, and Li Zhang. Dg-slam: Robust dy-  
647 namic gaussian splatting slam with hybrid pose optimization. In *Advances in Neural Information*  
*Processing Systems (NeurIPS)*, 2024a.

648 Zhen Xu, Sida Peng, Haotong Lin, Guangzhao He, Jiaming Sun, Yujun Shen, Hujun Bao, and Xi-  
649 aowei Zhou. 4k4d: Real-time 4d view synthesis at 4k resolution. In *Proceedings of the IEEE/CVF*  
650 *conference on computer vision and pattern recognition*, pp. 20029–20040, 2024b.

651  
652 Lixin Xue, Chen Guo, Chengwei Zheng, Fangjinghua Wang, Tianjian Jiang, Hsuan-I Ho, Manuel  
653 Kaufmann, Jie Song, and Otmar Hilliges. Hsr: holistic 3d human-scene reconstruction from  
654 monocular videos. In *European Conference on Computer Vision*, pp. 429–448. Springer, 2024.

655 Lihe Yang, Bingyi Kang, Zilong Huang, Zhen Zhao, Xiaogang Xu, Jiashi Feng, and Hengshuang  
656 Zhao. Depth anything v2. *arXiv:2406.09414*, 2024a.

657  
658 Ziyi Yang, Xinyu Gao, Wen Zhou, Shaohui Jiao, Yuqing Zhang, and Xiaogang Jin. Deformable  
659 3d gaussians for high-fidelity monocular dynamic scene reconstruction. In *Proceedings of the*  
660 *IEEE/CVF conference on computer vision and pattern recognition*, pp. 20331–20341, 2024b.

661 Richard Zhang, Phillip Isola, Alexei A Efros, Eli Shechtman, and Oliver Wang. The unreasonable  
662 effectiveness of deep features as a perceptual metric. In *Proceedings of the IEEE conference on*  
663 *computer vision and pattern recognition*, pp. 586–595, 2018.

664 Zetong Zhang, Manuel Kaufmann, Lixin Xue, Jie Song, and Martin R Oswald. Odhsr: Online dense  
665 3d reconstruction of humans and scenes from monocular videos. In *Proceedings of the Computer*  
666 *Vision and Pattern Recognition Conference*, pp. 21824–21835, 2025.

## 669 A THE REASON FOR NORMAL SUPERVISION

670  
671 Common forms of geometric supervision include depth and normal supervision. This work has  
672 tried both of these two methods and found the normal supervision is more useful in the end. There  
673 are two common types of mono depth supervisions, one is depth ordering loss, the other is pixel-  
674 wise difference loss. In the context of human–scene reconstruction, this work find that while exist-  
675 ing monocular depth estimation methods provide reliable relative depth ordering, it could provide  
676 such little benefit for SMPL-driven avatar optimization. Moreover, their per-pixel metric depth  
677 predictions remain unsatisfactory. The per-pixel depth supervision is so strict that this unsatisfactory  
678 prediction, combined with the additional inaccuracies introduced during scale alignment, can signif-  
679 icantly undermine the effectiveness of geometry optimization. In contrast, the inferred normal maps  
680 are usually much more reliable and provide valuable guidance for improving the avatar’s surface  
681 geometry.

682 In particular, even though color and normal rendering at the acting view of the avatar are reliable,  
683 there is no guarantee that the avatar is reconstructed with the correct spatial position in the scene.  
684 With the pinhole camera model, scaling the avatar by an arbitrary factor produces the same color and  
685 normal renderings in the camera coordinate system. To resolve the issue of scale ambiguity, it is es-  
686 sential to impose additional constraints that enforce contact between the avatar and the surrounding  
687 environment.

## 688 B THE REASON FOR SCALE SUPERVISION

689  
690 In particular, even though color and normal rendering at the acting view of the avatar are reliable,  
691 there is no guarantee that the avatar is reconstructed with the correct spatial position in the scene.  
692 With the pinhole camera model, scaling the avatar by an arbitrary factor produces the same color and  
693 normal renderings in the camera coordinate system. To resolve the issue of scale ambiguity, it is es-  
694 sential to impose additional constraints that enforce contact between the avatar and the surrounding  
695 environment.  
696

## 697 C THE USE OF LARGE LANGUAGE MODEL

698  
699 In accordance with the Policies on Large Language Model Usage at ICLR 2026, we hereby disclose  
700 that an LLM was utilized solely for improving the grammar and wording of this paper. The LLM  
701 was employed to refine the clarity and readability of the text, ensuring that the manuscript adheres to

702  
703  
704  
705  
706  
707  
708  
709  
710  
711  
712  
713  
714  
715  
716  
717  
718  
719  
720  
721  
722  
723  
724  
725  
726  
727  
728  
729  
730  
731  
732  
733  
734  
735  
736  
737  
738  
739  
740  
741  
742  
743  
744  
745  
746  
747  
748  
749  
750  
751  
752  
753  
754  
755

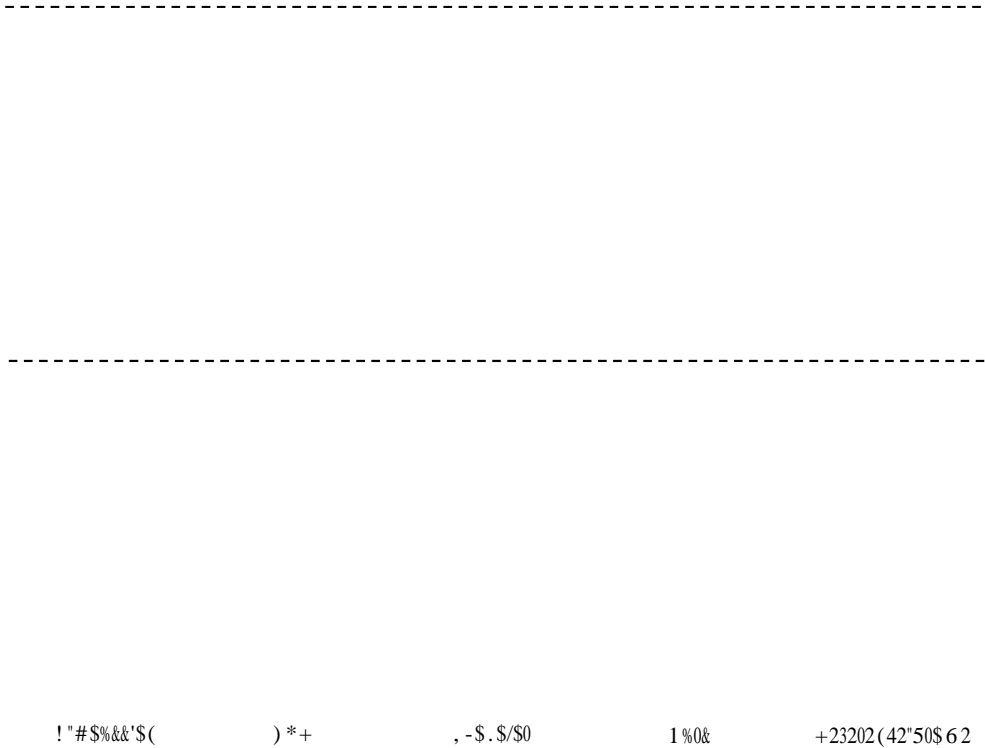


Figure 8: Qualitative Comparison at novel evaluation view with the baselines

high linguistic standards. We, the authors, take full responsibility for the content of this submission, ensuring that all claims, data, and results are accurate and free from misrepresentation.